

Deep learning-based framework for city-scale rooftop solar potential estimation by considering roof superstructures

Qingyu Li^a, Sebastian Krapf^b, Lichao Mou^a, Yilei Shi^c, Xiao Xiang Zhu^{a,d,*}

^a Data Science in Earth Observation, Technical University of Munich, Munich, 80333, Germany

^b Institute of Automotive Technology, Technical University of Munich, Garching, 85748, Germany

^c School of Engineering and Design, Technical University of Munich, Munich, 80333, Germany

^d Munich Center for Machine Learning, Munich, 80333, Germany

ARTICLE INFO

Keywords:

Convolutional neural network
Remote sensing
Roof superstructure
Solar potential
Local climate zone

ABSTRACT

Solar energy is an environmentally friendly energy source. Identifying suitable rooftops for solar panel installation contributes to not only sustainable energy plans but also carbon neutrality goals. Aerial imagery, bolstered by its growing availability, is a cost-effective data source for rooftop solar potential assessment at large scale. Existing studies generally do not take roof superstructures into account when determining how many solar panels can be installed. This procedure will lead to an overestimation of solar potential. Only several works have considered this issue, but none have devised a network that can simultaneously learn roof orientations and roof superstructures. Therefore, we devise SolarNet+, a novel framework to improve the precision of rooftop solar potential estimation. After implementing SolarNet+ on a benchmark dataset, we find that SolarNet+ outperforms other state-of-the-art approaches in both tasks — roof orientations and roof superstructure segmentation. Moreover, the SolarNet+ framework enables rooftop solar estimation at large-scale applications for investigating the correlation between urban rooftop solar potential and various local climate zone (LCZ) types. The results in the city of Brussels reveal that three specific LCZ urban types exhibit the highest rooftop solar potential efficiency: compact highrise (LCZ1), compact midrise (LCZ2), and heavy industry (LCZ10). The annual photovoltaic potential for these LCZ types is reported as 10.56 GWh/year/km², 11.77 GWh/year/km², and 10.70 GWh/year/km², respectively.

1. Introduction

With the accelerated urban expansion, it is expected that the urban population's share will rise to 68% in 2050 [1], introducing challenges such as growing energy demand and increasing greenhouse gas emissions [2]. To ensure sustainable development of the whole globe, the United Nations established 17 sustainable development goals (SDGs). SDGs have consolidated the UN member states' commitments to frame their economic, political, and environmental policies. Solar photovoltaic (PV) systems (e.g., solar panels) can convert sunlight into electricity, making solar power an inexhaustible and renewable energy source. Solar energy contributes to reducing greenhouse gas emissions and alleviating increasing energy demand [3]. Therefore, promoting solar energy corresponds to achieving SDG 7: Affordable and Clean Energy and SDG 13: Climate Action [4].

The rooftop is an optimal location for the installation of solar panels. One main advantage of rooftop-mounted solar panels is that no additional land is required. This is because some unused space on rooftops

can be leveraged [5,6]. Another advantage is that each building is able to gain a new role as an energy producer in addition to the former role as an energy consumer. This new role helps to avoid extensive transmission loss [7] and initiate net-zero energy buildings [8]. To formulate sustainable energy policies, an accurate assessment of rooftop solar potential is of utmost importance [9]. However, developing an effective framework that can identify suitable rooftops to install solar panels is still challenging, especially for large-scale applications [10].

Aerial imagery and airborne laser scanning (ALS) data are commonly used data sources for rooftop solar potential estimation. ALS data can effectively be used to calculate detailed rooftop geometry (e.g., slope and aspect) and enable the estimation of shading by vegetation and neighboring buildings [11]. However, in most countries, ALS data is often not publicly available. Alternatively, aerial imagery, bolstered by its growing availability, is a cost-effective data source for rooftop solar potential estimation.

* Corresponding author at: Data Science in Earth Observation, Technical University of Munich, Munich, 80333, Germany.

E-mail addresses: qingyu.li@tum.de (Q. Li), sebastian.krapf@tum.de (S. Krapf), lichao.mou@tum.de (L. Mou), yilei.shi@tum.de (Y. Shi), xiaoxiang.zhu@tum.de (X.X. Zhu).

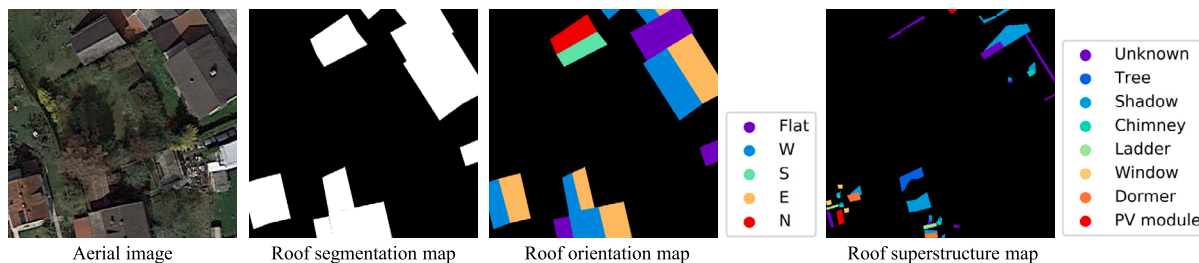


Fig. 1. Sample data for aerial imagery, roof orientation map, roof segmentation map, and roof superstructure map.

Mainstream strategies using aerial imagery fall back on two steps. They first extract the feasible rooftop areas for solar panel placement and then estimate solar potential. Most methods extract roof segmentation maps (see Fig. 1) using convolutional neural networks (CNNs) for the first step [12–14]. Nevertheless, the orientations and tilts of roof segments are often disregarded, resulting in either an overestimation or underestimation of solar potential. To address this, some studies [15,16] and our former SolarNet framework [17] propose to learn the roof orientation map (see Fig. 1) that characterizes roof segments and their orientations. The orientation of the roof segment determines received solar irradiation, which exerts a great impact on the generated solar energy [18].

Nevertheless, these above studies and SolarNet [17] have neglected one point: some portions of the roof area may be unavailable for solar system installation due to obstructions [19–22] such as windows or chimneys, which are known as superstructures. Therefore, before calculating the number of solar panels that can be accommodated within the specific roof shape, we also need to extract roof superstructures. Our work considers both roof orientations and roof superstructures in the assessment of solar potential. In this way, we can not only pinpoint optimal sites for solar installations but also prevent an overestimation of solar potential.

Therefore, we propose SolarNet+, a framework that learns roof orientations and roof superstructures using a CNN, followed by the assessment of solar potential. Moreover, we observe existing studies fail to learn roof orientations and roof superstructures simultaneously [23,24]. Thus, we devise an innovative multi-task learning network that is capable of learning both roof orientation maps and roof superstructure maps simultaneously. Specifically, roof segmentation masks are initially learned and allocated on contextual and multi-scale features for further learning of roof orientations and superstructures. By doing so, not only can the building roof information be enhanced, but background clutters such as cars and roads can also be suppressed.

The local climate zone (LCZ) scheme, introduced by [25], is crafted to create a uniform classification system for examining urban climate characteristics, e.g., temperature, humidity, and wind patterns. These urban climate characteristics can also impact the effectiveness of solar panels. For example, higher temperatures will reduce the electrical efficiency of PV modules [26,27]. Moreover, LCZ classification is determined by considering land surface cover and building type cover, with each building type corresponding to different energy requirements. Integrating the LCZ concept into building energy research allows us to examine rooftop solar potential concerning the local urban form and microclimate. However, there is a lack of current research exploring the rooftop solar potential based on the LCZ scheme. This paper analyzes and assesses the correlation between the solar potential on urban rooftops and various LCZ types. Notably, this study is pioneering in applying deep learning methods to investigate the connection between rooftop solar potential and LCZ.

Our work presents three main contributions:

(1) We devise SolarNet+, a novel framework for estimating rooftop solar potential from aerial images for large-scale applications. The code of the SolarNet+ framework will be made publicly available in https://github.com/lqycrystal/SolarNet_plus.

(2) Experimental results suggest that our framework is superior to other competitors in terms of not only the prediction accuracy of roof orientations and superstructures but also the estimation precision of rooftop solar potential.

(3) We investigate the relationship between LCZ and rooftop solar potential. This helps to augment the alignment of the potential utilization of solar energy and urban planning.

2. Methodology

2.1. Pipeline

Fig. 2 shows the pipeline of the SolarNet+ framework. The input aerial image is fed into a CNN to learn roof orientation and superstructure maps. Based on the predicted roof orientation map, individual classes of roof segments (*i.e.*, Flat, west (W), south (S), east (E), and north (N)) are extracted, and their roof area available for solar panel installation is derived by excluding the area of superstructures, which is determined using the predicted roof superstructure map. The yearly generated energy per solar panel can be obtained from a solar radiation database for each roof segment category. Next, this value is multiplied by the maximum number of solar panels installed on roof segments. Ultimately, the overall rooftop solar potential is calculated by aggregating the potential across all categories of roof segments.

2.2. Extraction of roof orientations and roof superstructures

Roof orientation is an important element in assessing solar potential, as it determines the amount of received solar irradiation. For instance, in northern hemisphere regions, a roof segment facing south generates 50% considerably more annual energy than one facing north [23]. Moreover, we must consider roof superstructures to prevent an overestimation of solar potential. This is essential because areas occupied by roof superstructures cannot accommodate new solar panels. Therefore, the first step of the SolarNet+ framework is to extract both roof orientations and roof superstructures from the input aerial imagery. Roof orientation extraction refers to segmenting roof segments according to their corresponding orientations. Roof superstructure extraction aims to segment individual classes of roof superstructures. Thus, we devised a multi-task learning network [17] for the SolarNet+ framework. It first learns the roof segmentation map that characterizes entire roof outlines. Next, the roof segmentation map is allocated to extracted features in order to learn roof orientation map and roof superstructure map. By doing so, not only background noise is reduced but also roof regions are enhanced.

The proposed network learns roof segmentation map, roof orientation map, and roof superstructure map. The objective function \mathcal{L} of our network is:

$$\mathcal{L} = \lambda \cdot \mathcal{L}_a + \alpha \cdot \mathcal{L}_b + \omega \cdot \mathcal{L}_c,$$

where \mathcal{L}_a , \mathcal{L}_b , and \mathcal{L}_c are based on cross-entropy loss functions used for optimizing the learning process of roof segmentation map, roof orientation map, and roof superstructure map, respectively. λ , α , and ω are hyperparameters to regulate the significance of each term. Empirically, we set λ as 0.1, α as 1, ω as 1.

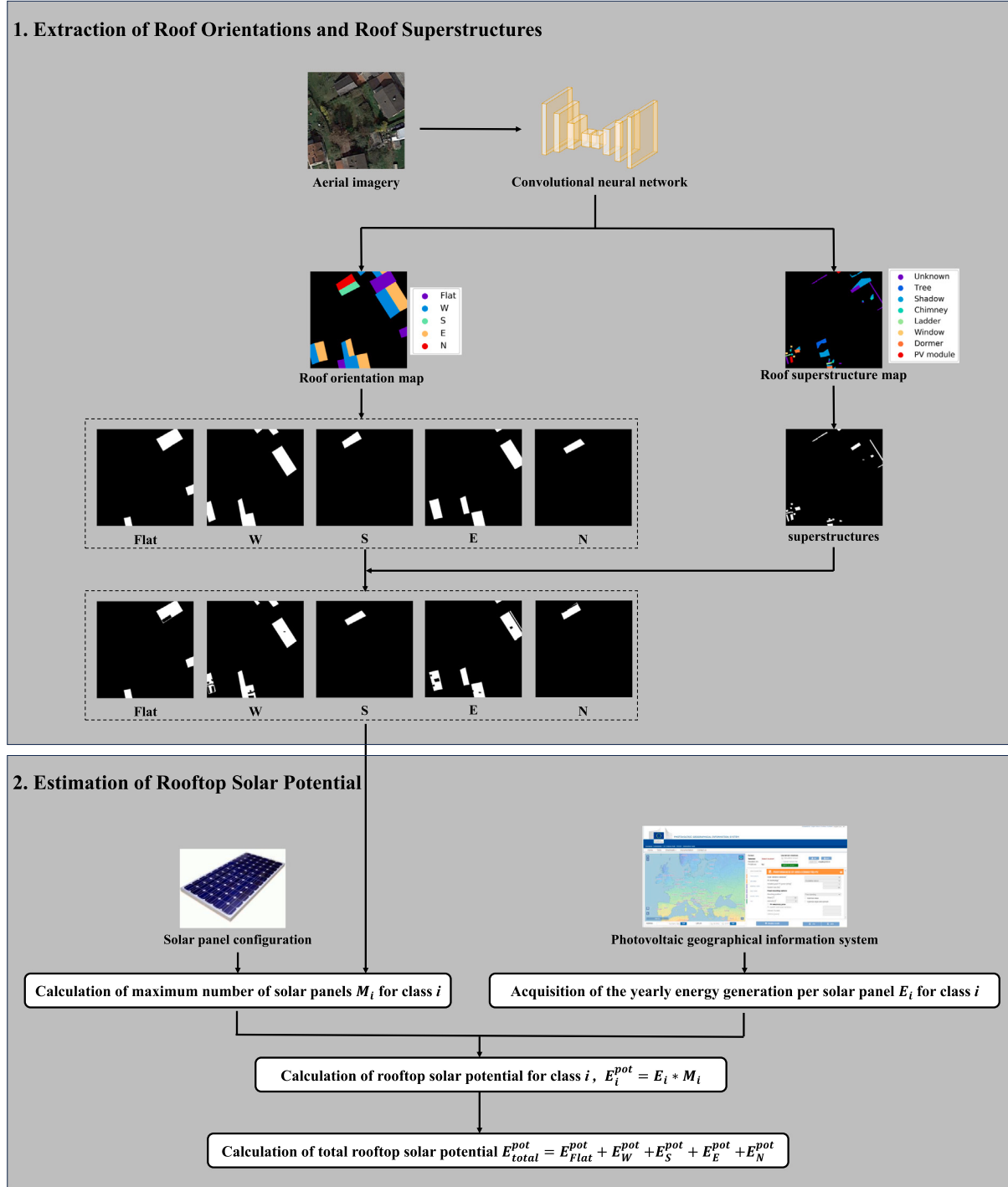


Fig. 2. The flowchart of the proposed SolarNet+ framework.

2.3. Estimation of rooftop solar potential

The assessment of rooftop solar potential in this study primarily concentrates on technical potential, *i.e.*, the energy generated by solar panels that are mounted on each roof segment. Here, we use a solar panel that has a size of 1.7 m in length and 1 m in width. Its peak power is 400 Wp. Given the slope and azimuth of the roof segment, the annual energy (Wh/year) generated by solar panels can be obtained by calling the PVGIS API [28]. Specifically, the yearly energy generation per solar panel E_i is derived from a look-up table of PVGIS [28]. Here, i refers to the corresponding class of roof segments that are either azimuth classes (W, S, E, and N) or flat roofs. The slope is defined as

30° for non-flat classes, corresponding to an approximation of the mean slope of buildings in South Germany [9]. Another crucial element for solar potential estimation is M_i which denotes the maximum number of mounted solar panels per type of roof segment. For the class i , the rooftop solar potential E_i^{pot} (Wh/year) is calculated as

$$E_i^{pot} = E_i * M_i.$$

With a summation of the potential of all classes, the total solar potential E_{total}^{pot} can be derived as

$$E_{total}^{pot} = E_{Flat}^{pot} + E_W^{pot} + E_S^{pot} + E_E^{pot} + E_N^{pot}.$$

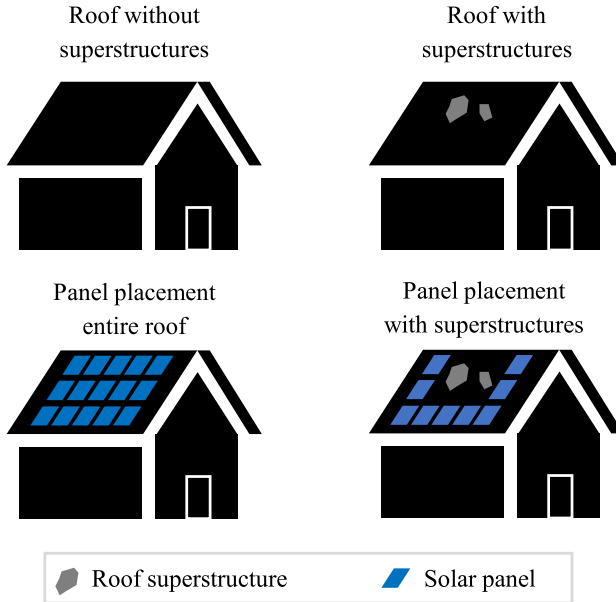


Fig. 3. Examples of solar panel placement on entire roof and roof with superstructures.

In what follows, we explain how to calculate M_i , a key element for assessing solar potential. First, both the learned roof orientation maps and roof superstructure maps obtained are converted into a vector format. The small roof segments that are less than 5 m^2 are deleted, as they are not appropriate for mounting solar panels. Afterward, we start to install solar panels on each roof segment. In this study, we adopted a horizontal-left packing technique to fill PV panels on rooftops. Panels are placed starting from the bottom left corner of each roof segment until the entire segment is filled up. If panels intersect with superstructures or the segment outline, they will be removed (c.f. Fig. 3). Note that for flat roofs, panels are placed in the south orientation, and neighboring panels have space in between to avoid shadowing themselves.

Fig. 4 shows an example of estimated solar potential when different factors are taken into account. The first case is the solar potential of the entire roof. Roof superstructures are considered in the second case, as the areas occupied by superstructures are not included in the assessment. The last case is more adherent to practical applications where both roof superstructures and the placement of solar panels are involved. The variances among different cases demonstrate the superiority of the SolarNet+ framework. This is because the SolarNet+ framework considers the orientation of roof segments, roof superstructures, and placement of solar panels, allowing a more precise estimation, while previous studies (e.g., the SolarNet framework [17]) fail to these factors into account.

3. Experiments

3.1. Data

To our knowledge, only one public dataset, *i.e.*, Roof Information Dataset (RID) [24] is available for the extraction of both roof segments and superstructures from aerial imagery. The dataset comprises annotations for roof segments and superstructures for 1880 buildings at a pixel-wise level. Regarding the roof orientation map, it encompasses six classes, including background, flat roof, and four azimuth classes corresponding to the orientation of the roof segment: W, S, E, and N. As for the roof superstructure map, nine classes are defined: background, unknown, tree, shadow, chimney, ladder, window, dormer, and PV module. The dataset is divided into training, validation, and test sets with a ratio of 7:1:2.

3.2. Experiment setup

In this study, we validate the SolarNet+ framework from two aspects. One is the comparison between SolarNet+ with other methods that can learn roof orientations and superstructures. The other is the investigation of the effect of different classes of rooftop superstructures on rooftop solar potential.

For a comprehensive evaluation of the results of roof orientations and superstructures, SolarNet+ is compared with several state-of-the-art methods. Specifically, concerning roof orientations, comparisons are made with five networks: DeepLab V3+ [33], FC-DenseNet [34], Efficient-UNet [35], U-Net [29], and SolarNet [17]. For roof superstructure, we perform comparisons with four semantic segmentation networks, DeepLab V3+ [33], FC-DenseNet [34], Efficient-UNet [35], and U-Net [29]. Moreover, for evaluating the performance of SolarNet+ in both roof orientations and roof superstructure extraction, multi-task learning approaches proposed by [30,32], and [31] are considered as competitors. In the context of rooftop solar potential estimation, we also conduct assessments involving these methods.

3.3. Accuracy assessment

We assess the model performance based on three aspects, *i.e.*, the accuracy of roof orientation prediction, the accuracy of roof superstructure prediction, and the precision of solar potential estimation.

3.3.1. Prediction accuracy of roof orientations and superstructures

To assess the accuracy of the predicted roof orientations and superstructures, mean intersection over union (mIoU) and overall accuracy (OA) are utilized as the evaluation criterion [17]. Note that a larger value suggests higher accuracy. IoU is first calculated for each class with the following equation:

$$\text{IoU} = \frac{TP}{TP + FP + FN}, \quad (1)$$

where FN , FP , and TP indicate the numbers of false negatives, false positives, and true positives, respectively. Next, mIoU is derived by averaging the IoU metrics of all classes. OA denotes the percentage of pixels that are correctly classified.

3.3.2. The estimation precision of rooftop solar potential

To evaluate the estimation precision of rooftop solar potential, we derive the amount of solar potential and the number of solar panels by leveraging the predicted roof orientation map and roof superstructure map from different deep networks. Moreover, the ground reference values are derived on the basis of the ground reference roof orientation map and roof superstructure map.

Furthermore, root mean squared error (RMSE) and percent root mean squared error (%RMSE) are introduced as the accuracy metric for solar potential estimation [36]. They are defined as:

$$\text{RMSE} = \sqrt{\frac{1}{n} \sum_{j=1}^n (P_j - \hat{P}_j)^2}, \quad (2)$$

$$\% \text{RMSE} = \frac{\sqrt{\frac{1}{n} \sum_{j=1}^n (P_j - \hat{P}_j)^2}}{\frac{1}{n} \sum_{j=1}^n P_j}, \quad (3)$$

where \hat{P}_j and P_j are estimated and ground reference solar potential values of j th image, respectively, and n represents the total count of images that need to be evaluated. Note that a smaller value of RMSE or %RMSE refers to higher precision. According to [36], model accuracy was deemed excellent when the %RMSE was less than 10%, good when the %RMSE was between 10% and 20%, fair when the %RMSE was between 20% and 30%, and poor when the %RMSE exceeded 30%. Here, the ground reference rooftop solar potential is derived based on the ground reference roof orientation map and roof superstructure map, while the estimated solar potential is obtained from the predicted roof orientation map and roof superstructure map from the deep network.

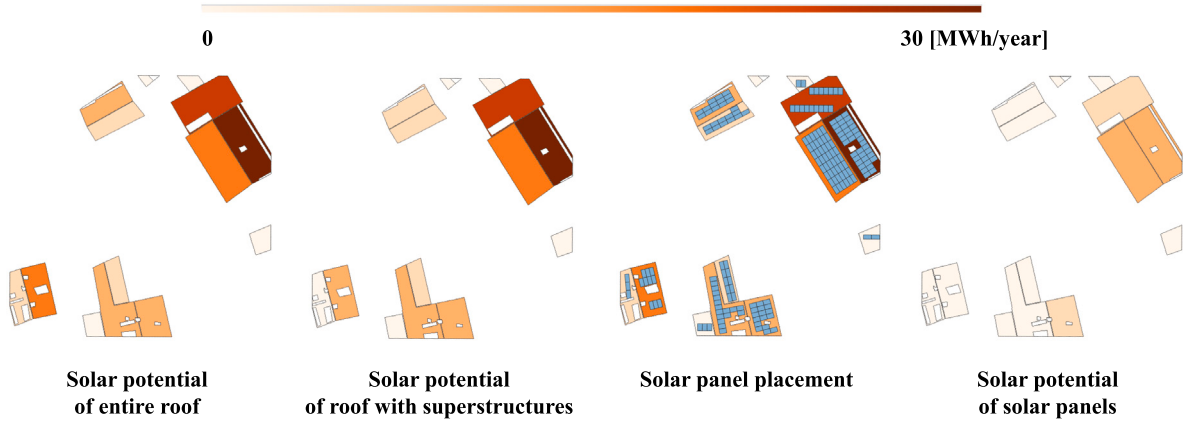


Fig. 4. Examples of rooftop solar potential estimation. The corresponding aerial imagery, roof orientation map, roof segmentation map, and roof superstructure map are in [Fig. 1](#).

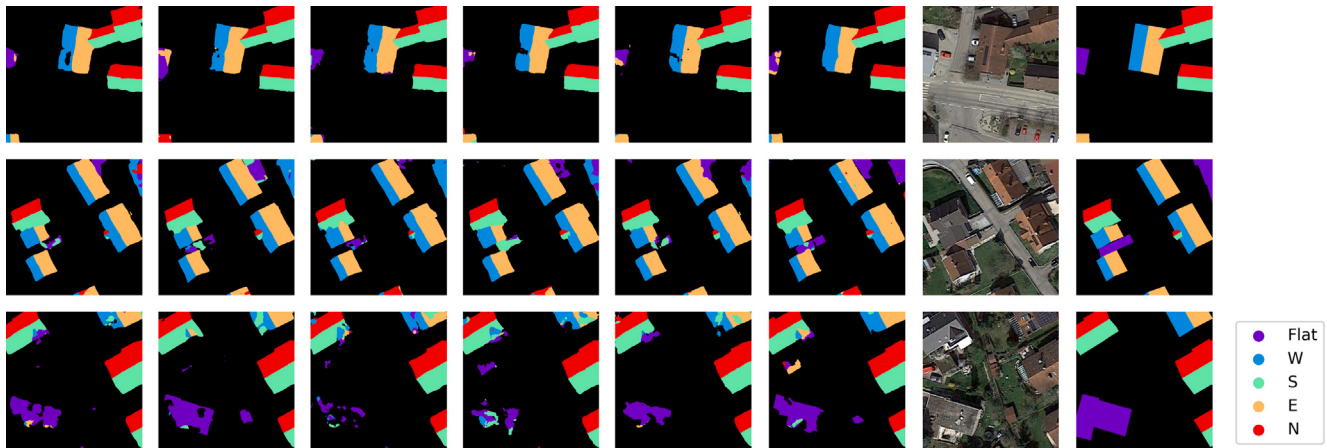


Fig. 5. From the left to right are results obtained by approaches proposed in U-Net [29], SolarNet [17], Srivastava et al. [30], Bischke et al. [31], Mou & Zhu [32], and SolarNet+ (our study). The last three columns are aerial images, the ground reference roof orientation maps, and their legend from the RID dataset.

4. Results

4.1. Results of roof orientation and roof superstructure prediction

[Table 1](#) reports accuracy metrics on the test set of the RID dataset. SolarNet+ outperforms all competitors in accuracy metrics of both roof orientations and roof superstructure. In comparison with single-task learning methods, our method achieves higher accuracy in terms of both two types of metrics. This demonstrates the satisfactory performance of multi-task learning. Besides, SolarNet+ also obtains increments in mIoU and OA when compared to other multi-task learning methods, indicating the effectiveness of our approach.

[Tables 2](#) and [3](#) report the results of individual classes in roof orientations and roof superstructures, respectively. It can be observed accuracy variances exist in different classes. For example, the classes of “Flat”, “W”, and “E” have lower IoU than other classes in general. Compared to other approaches, SolarNet+ has shown higher IoU in these classes. For the task of roof superstructure extraction, “Tree” and “Ladder” have relatively lower IoU than other classes. Nevertheless, SolarNet+ can contribute to the improvement of IoU with respect to these two classes.

[Fig. 5](#) presents several examples of roof orientation maps produced by different methods. Unlike other competitors, our approach exhibits a reduced tendency to misclassify “Flat” as other classes. Moreover, [Fig. 6](#) presents roof superstructure maps generated by different approaches. The outcomes obtained from SolarNet+ more closely align with the ground reference.

4.2. Results of solar potential estimation

To roughly gauge the impact of roof superstructures on roof solar potential estimation, we have investigated the amount of solar potential and the number of solar panels using ground reference data with roof superstructures and those without roof superstructures. According to the calculation on the test set of the RID dataset (see [Table 4](#)), when not considering roof superstructures, the overestimation of the number of solar panels and the amount of solar potential is evident.

Moreover, we also present the quantitative results of the solar potential estimation obtained by different networks (see [Table 5](#)). Specifically, we calculate the number of solar panels that can be installed and the amount of solar potential that can be obtained on the basis of predicted roof orientations and superstructures. The metrics derived from SolarNet+ are closer to those derived by ground reference roof orientation maps and roof superstructure maps. Moreover, when compared to other deep networks, SolarNet+ has the lowest value in RMSE. The estimation precision ($\%RMSE = 19.92$) of the SolarNet+ framework suggests our framework has achieved good results in solar potential assessment.

[Fig. 7](#) shows the result of applying the SolarNet+ framework at a larger scale, which demonstrates applying the proposed framework is promising in real cases. Lighter-colored roof segments indicate a lower estimated solar potential.

4.3. Transferability of SolarNet+

In this research, SolarNet+ is applied to the RID dataset that is collected from Wartenberg. As Wartenberg is a small city, we want

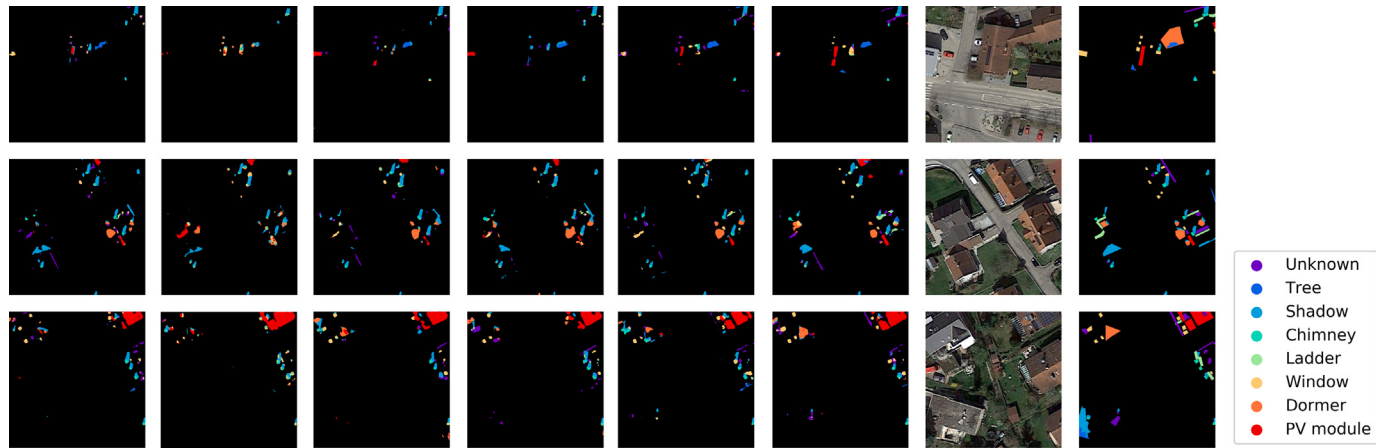


Fig. 6. From the left to right are results obtained by approaches proposed in U-Net [29], FC-DenseNet [34], Srivastava et al. [30], Bischke et al. [31], Mou & Zhu [32], and SolarNet+ (our study). The last three columns are aerial images, the ground reference roof superstructure maps, and their legend from the RID dataset.

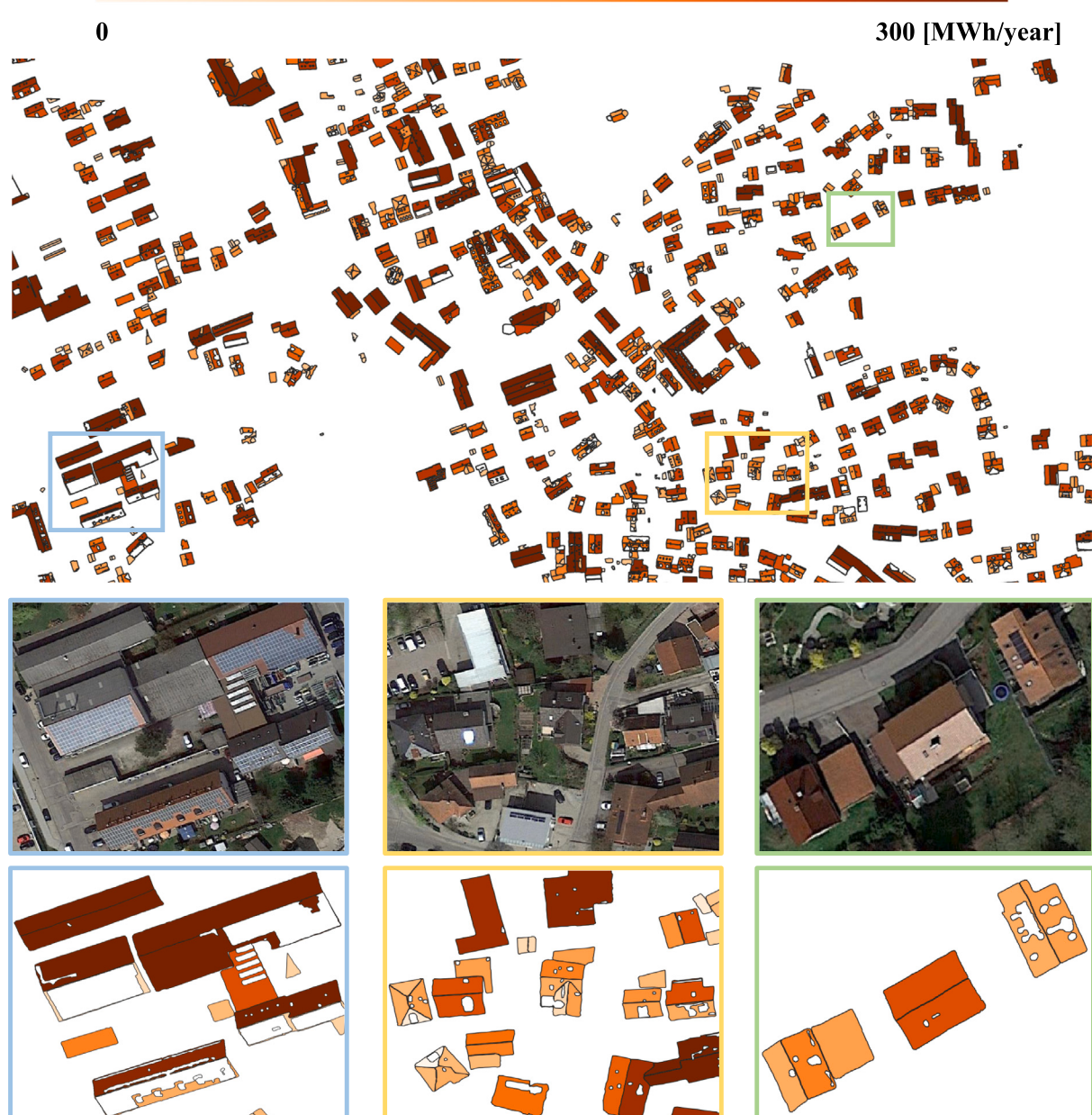


Fig. 7. Example estimated results of rooftop solar potential in an area of the city of Wartenberg.

Table 1
Accuracy metrics of different networks on RID dataset. (%)

Type of learning	Method	Roof orientations		Roof superstructures	
		mIoU	OA	mIoU	OA
Single-task	U-Net [29]	73.41	95.01	35.07	97.69
	FC-DenseNet [34]	68.05	93.86	26.74	97.44
	Efficient-UNet [35]	66.67	93.59	23.93	96.88
	DeepLab V3+ [33]	44.89	87.57	16.69	96.65
	SolarNet [17]	75.38	95.47	-	-
	Srivastava et al. [30]	71.69	94.70	33.97	97.63
Multi-task	Bischke et al. [31]	71.91	94.78	35.28	97.68
	Mou & Zhu [32]	71.65	94.73	36.70	97.71
	SolarNet+	75.69	95.52	36.72	97.84

Table 2
IoU of individual classes of roof orientations that are obtained from different semantic segmentation networks on the RID dataset. (%) BG is the class of Background.

Method	BG	Flat	W	S	E	N
U-Net [29]	96.20	42.42	66.02	79.36	74.02	82.43
FC-DenseNet [34]	95.58	30.79	61.92	74.42	68.56	77.03
Efficient-UNet [35]	95.24	32.08	57.76	73.05	66.24	75.66
DeepLab V3+ [33]	92.65	13.69	31.29	46.71	35.36	49.61
SolarNet [17]	96.67	46.07	68.44	80.95	76.75	83.40
Srivastava et al. [30]	95.98	37.63	63.80	77.42	73.80	81.69
Bischke et al. [31]	96.08	38.16	63.89	77.91	73.57	81.89
Mou & Zhu [32]	96.01	35.67	64.57	78.37	72.95	82.37
SolarNet+	96.62	46.28	69.02	80.45	78.35	83.41

Table 3
IoU of individual classes of roof superstructures that are obtained from different semantic segmentation networks on the RID dataset. (%) BG is the class of Background.

Method	BG	Unknown	Tree	Shadow	Chimney	Ladder	Window	Dormer	PV module
U-Net [29]	97.88	11.78	1.59	32.25	38.14	7.11	32.40	26.63	67.88
FC-DenseNet [34]	97.77	0.15	0.03	25.93	25.38	0.00	18.82	14.83	57.78
Efficient-UNet [35]	97.31	7.72	1.48	23.42	2.18	1.95	16.99	12.71	51.49
DeepLab V3+ [33]	96.79	0.18	0.00	14.70	0.00	0.00	0.23	0.03	38.26
Srivastava et al. [30]	97.89	12.04	4.61	29.48	30.98	6.65	30.47	29.11	64.46
Bischke et al. [31]	97.93	13.22	3.44	29.80	34.26	12.71	33.82	28.43	63.91
Mou & Zhu [32]	97.95	12.98	7.01	31.40	37.92	10.43	33.07	32.04	67.57
SolarNet+	98.14	14.45	9.26	33.05	21.80	7.92	36.61	39.92	69.32

Table 4
Impact of roof superstructures of rooftop solar potential using the ground reference data on the RID dataset.

If considering roof superstructures	Number of solar panels that can be installed	Amount of solar potential that can be obtained (Mwh/year)
Yes	24279	7959.76
No	34466	11411.33

Table 5
Quantitative results of rooftop solar potential on the RID dataset.

Method	Number of solar panels that can be installed	Amount of solar potential that can be obtained (Mwh/year)	RMSE (Mwh/year)	%RMSE
U-Net [29]	25855	8484.28	12.77	21.49
FC-DenseNet [34]	29316	9544.90	20.85	35.10
Efficient-UNet [35]	23842	7754.68	16.85	28.37
DeepLab V3+ [33]	28152	9153.37	25.14	42.32
Srivastava et al. [30]	24987	8125.64	12.63	21.27
Bischke et al. [31]	25749	8446.82	14.34	24.13
Mou & Zhu [32]	24945	8075.86	14.22	23.93
SolarNet+	24541	7967.34	11.83	19.92
Ground reference	24279	7959.76	-	-

Table 6
Quantitative results of rooftop solar potential on Munich.

Method	Number of solar panels that can be installed	Amount of solar potential that can be obtained (Mwh/year)	RMSE (Mwh/year)	%RMSE
SolarNet+	28560	9594.67	7.90	17.10
Ground reference	29641	9977.61	-	-

to investigate the transferability of SolarNet+ in other geographical regions where rooftops show diverse structural appearances. Therefore,

we plan to test the applicability of SolarNet+ in the areas where buildings are dissimilar from those in Wartenberg. In this regard, we collect

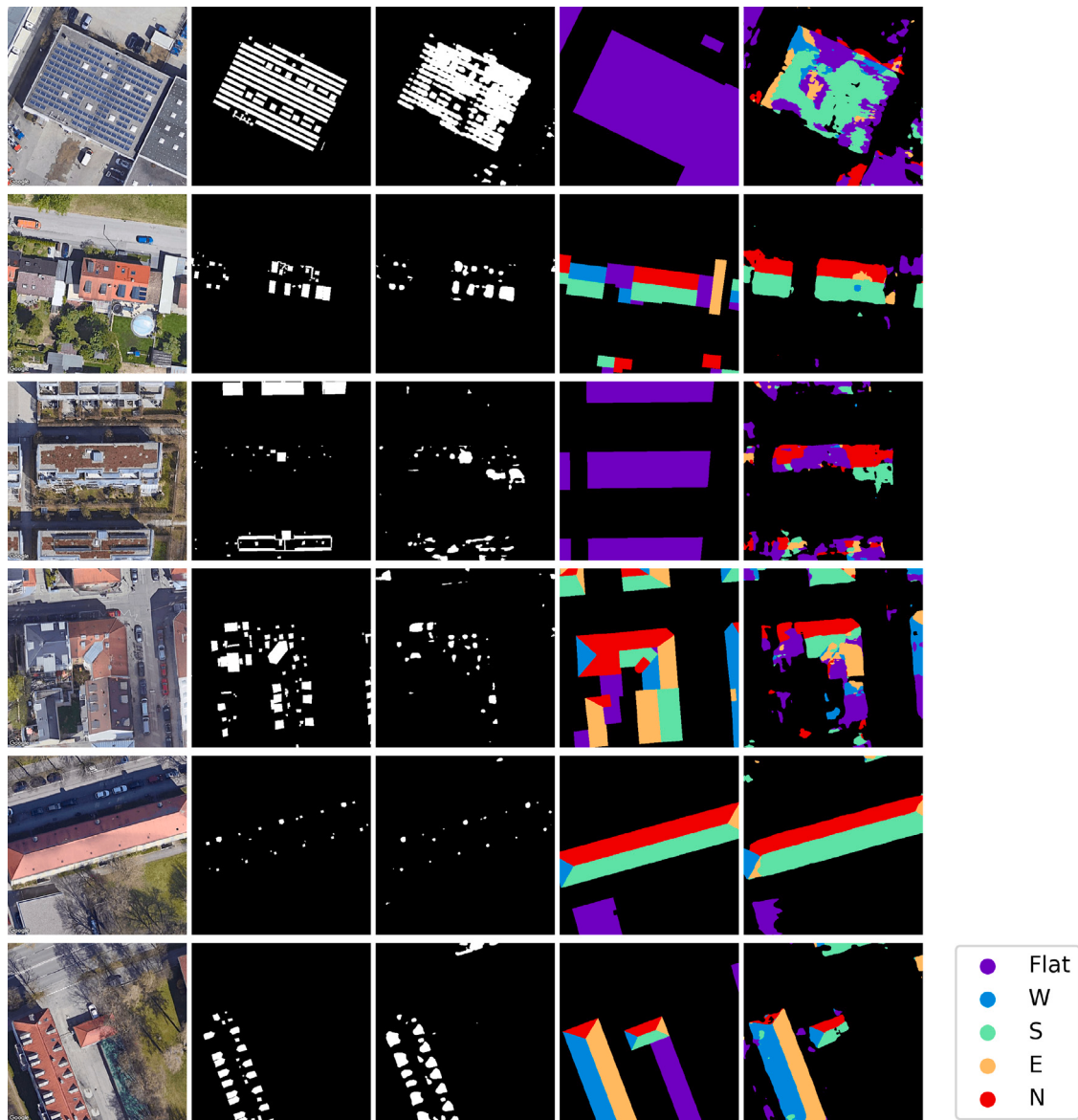


Fig. 8. Prediction results on Munich. Columns from left to right are: aerial images, ground reference masks of roof superstructures, predicted masks of roof superstructures, ground reference masks of roof orientations, predicted masks of roof orientations, and legend.

samples (216 buildings) from the urban area in Munich. The ground reference roof orientation maps are derived by the method in [16], while the ground reference roof superstructure maps are annotated manually.

Roof superstructures are vital to rooftop solar potential estimation, as new solar panels cannot be installed in areas where the roof superstructures are located. Existing methods [23,24] learn roof superstructure map consisting of 9 classes: 8 types of superstructures as well as background class. However, it can be observed some classes of superstructures (e.g., air conditioner and balcony) are not involved in this representation (see Fig. 8 in Munich). The representation consisting of 9 classes is burdened with not only the missing categories of superstructure but also a large volume of work for data annotation. Therefore, we investigate another representation encompassing 2 classes that depict roof superstructures. For this representation, we combine all superstructures as one class. In other words, two classes, including superstructure and non-superstructure, are defined in this representation.

Specifically, we train the model with the RID dataset and then evaluate it on test instances collected from the urban area in Munich.

The transferability of SolarNet+ can be evaluated from both qualitative and quantitative perspectives. Fig. 8 illustrates the visual results of the roof superstructure and roof orientation. With respect to numerical results, the IoU metrics of roof superstructure and roof orientation prediction are 20.80% and 23.86%, respectively. The estimation precision of rooftop solar potential is shown in Table 6, suggesting the transferability of SolarNet+. Of course, there is still a large space to be improved. However, considering the rooftops are largely different between Wartenberg and Munich, the achieved results are already impressive. As shown in the first two rows of Fig. 8, SolarNet+ is able to extract roof superstructures such as “PV module” and “Dormer” well. However, SolarNet+ fails to segment some superstructures in some cases. This phenomenon is attributed to two reasons. On the one hand, there are significant differences in the type of roof superstructures. For example, the balconies in Munich (c.f. the third row of Fig. 8) have not been extracted by SolarNet+, as the class of balcony is not included in the RID dataset. On the other hand, the material, color, and size of building rooftops are divergent, which also introduces great challenges. For future research, we aim to collect more training samples from a wide range of cities. This helps to increase the rooftop's style diversity, contributing to the amplexness of rooftop samples.

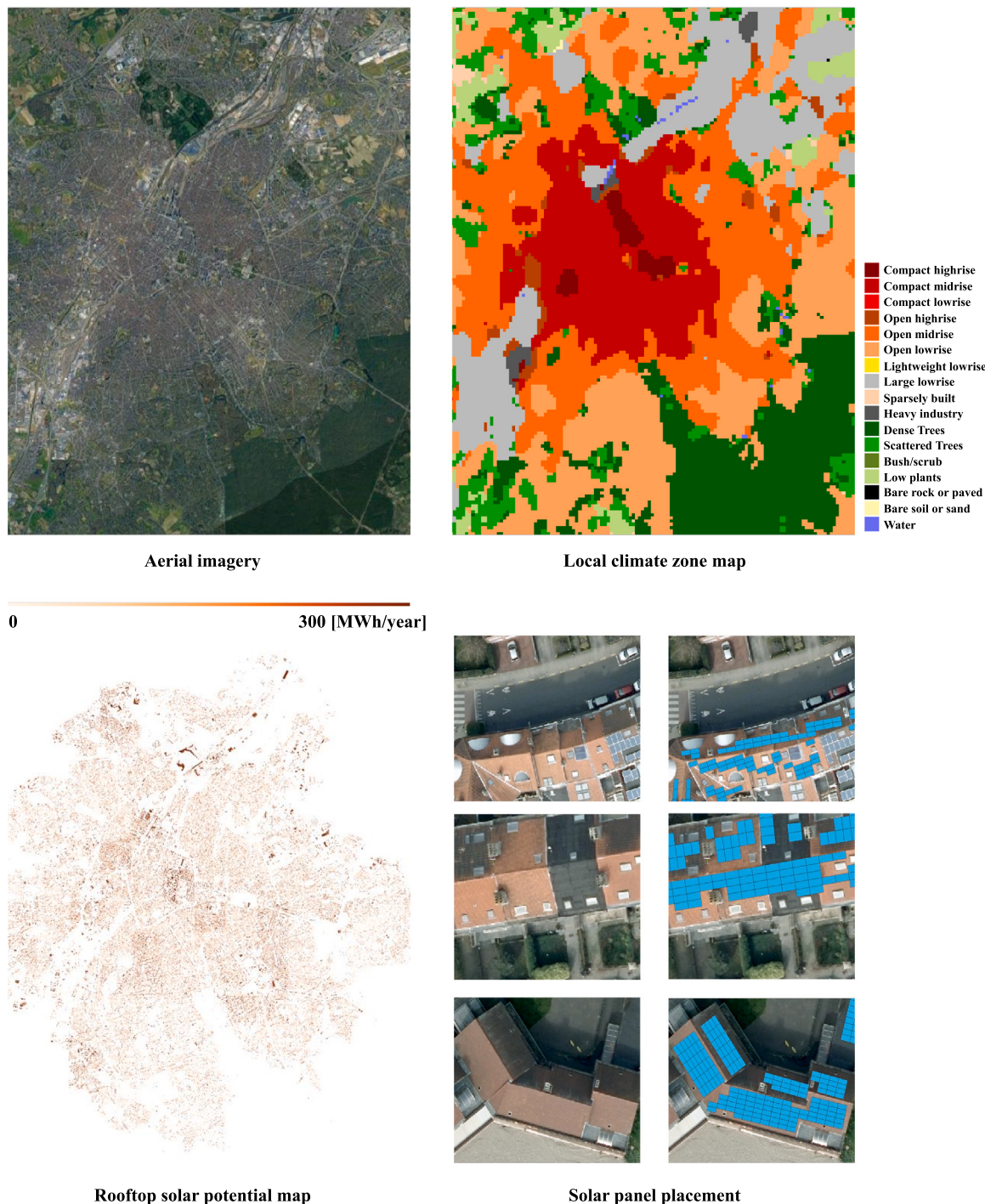


Fig. 9. Rooftop solar potential results derived from the SolarNet+ framework and local climate zone map in the city of Brussels.

5. Rooftop solar potential of different LCZs

Considering the availability of very high-resolution aerial imagery and similar structural appearances of buildings with German cities, the city of Brussels in Belgium is selected as the study area for investigating rooftop solar potential in different LCZs. Specifically, we train the model with the RID dataset and then infer aerial imagery (spatial resolution: 0.1 m/pixel) collected from Brussels <https://datastore.brussels/web/urbis-download>. Afterward, the rooftop solar potential (see Fig. 9) is estimated by using the predicted roof orientation maps and roof superstructure maps from the SolarNet+ framework. Moreover, we

illustrated the solar placement strategy (solar panels in blue) from the derived results in Fig. 9.

The LCZ scheme, introduced by [25], is a classification framework that divides urban areas into distinct zones based on their surface characteristics, including surface cover (pervious or impervious surfaces), as well as building height and density. The LCZ system comprises 17 standard classes comprising 10 built types (LCZ 1-10) and 7 land cover types (LCZ A-G). Each LCZ class corresponds to specific urban climate characteristics with distinct influence on the efficiency of solar panels and building energy performance patterns. Therefore, in this study, we adopt the LCZ scheme as a spatial framework to analyze

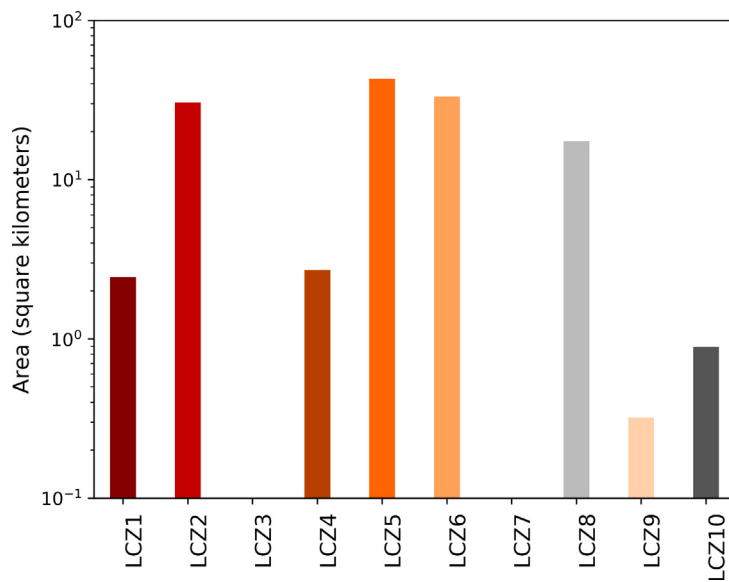


Fig. 10. Distribution of local climate zone (LCZ) urban classes in the city of Brussels.

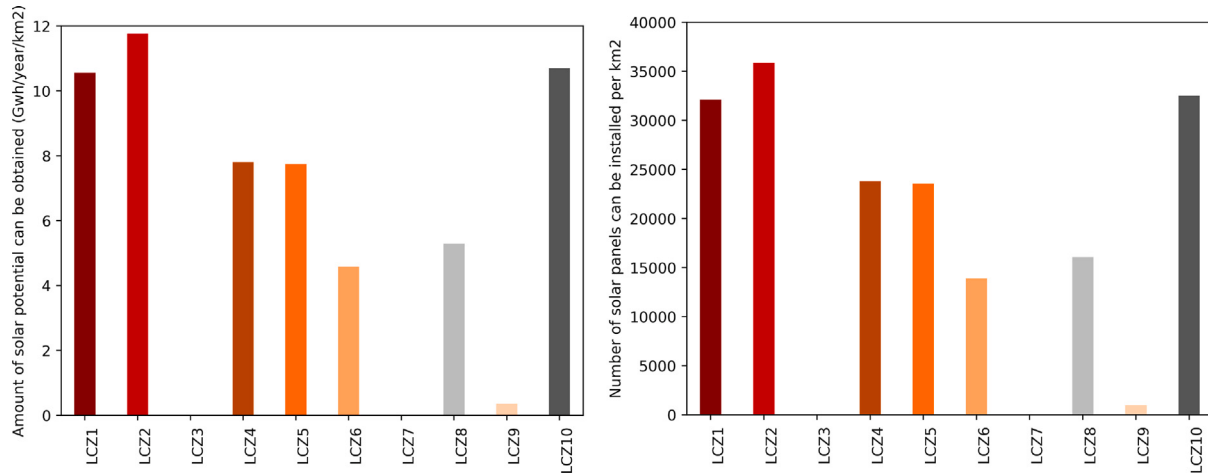


Fig. 11. The amount of solar potential per km^2 that can be obtained and the number of solar panels per km^2 that can be installed per year in each local climate zone class.

the relationship between urban form characteristics and rooftop solar potential.

The LCZ map utilized in this study is a global dataset [37] presenting LCZ categories at a spatial resolution of 100 meters per pixel, derived from Sentinel-1, Sentinel-2, and Landsat data collected in 2018. Fig. 10 presents the distribution of the LCZ urban classes of Brussels. The most prevalent urban classes are compact midrise (LCZ2), open midrise (LCZ5), and open lowrise (LCZ6). LCZ2 is characterized mainly by tightly packed buildings of 3 to 9 stories. LCZs 5 and 6 exhibit a greater presence of green space compared to LCZ2, and the buildings in these zones are less densely clustered. LCZs 3 and 7, representing compact lowrise and lightweight lowrise were notably scarce or absent in the analyzed data.

Additionally, the annual amount of rooftop solar potential per km^2 can be obtained and the number of solar panels per km^2 that can be installed for various LCZ types in Brussels are computed. As depicted in the results presented in Fig. 11, the most significant contributor to annual PV power generation per km^2 is compact groups (LCZ1 and LCZ2), mixed-use urban environments with highrise and midrise structures, such as apartments, offices, and commercial buildings, reaching 10.56 GWh/year/ km^2 and 11.77 GWh/year/ km^2 , respectively. Following closely is heavy industry (LCZ10) which characterizes low-rise and

mid-rise industrial structures, generating 10.70 GWh annually per km^2 . These results inform more efficient energy planning and utilization, allowing for targeted strategies in areas with higher solar potential.

6. Discussion

In this research, remote sensing imagery collected from airborne sensors is utilized as the input data for SolarNet+. This ensures it can maintain precision and accuracy across different scales, from small neighborhoods to larger urban areas, and potentially even at regional scales.

Neighborhood Scale: Our framework can offer detailed analyses of individual rooftops, allowing homeowners to make informed decisions about solar panel installations. The model's ability to generate accurate roof orientation and superstructure maps ensures that even small variations in rooftop structures are accounted for, optimizing the solar potential estimation for each building at the neighborhood scale.

City Scale: SolarNet+ framework can provide comprehensive insights into the overall solar capacity of the entire city by aggregating the results from individual buildings. This makes SolarNet+ a powerful tool for assessing the solar potential at the city scale, contributing to developing city-wide renewable energy strategies.

Regional Scale: The proposed framework can also be extended to regional applications. For instance, regional planning authorities are able to optimize the deployment of solar infrastructure across diverse landscapes based on large-scale results. However, acquiring the necessary datasets is a significant challenge for similar large-scale applications. This issue can be addressed by utilizing alternative remote sensing data sources. For instance, commercial satellites such as Albedo provide remote sensing imagery with very high spatial resolution (0.1 m/pixel). This satellite constellation theoretically covers the entire globe and is more cost-effective compared to aerial imagery. Despite this, the expense associated with such high-resolution data remains prohibitive for applications at national, continental, or global scales.

In summary, the SolarNet+ framework is adaptable and capable of providing solar potential estimation across various scales, from individual neighborhoods to entire regions. Our framework can be a valuable tool for a wide range of stakeholders involved in the transition to renewable energy due to its flexibility.

7. Conclusion and outlook

The energy generated through rooftop-mounted solar panels is able to compensate for the growing energy demand and greenhouse gas emissions. Accurate estimation of rooftop solar potential is vital to formulating policies related to sustainable energy planning and carbon reduction. Therefore, we devise SolarNet+, a novel framework that estimates rooftop solar potential by identifying suitable areas for solar panel installation on roofs. Our framework involves two parts: (a) a multi-task learning network that learns roof orientation maps and roof superstructure maps from aerial images, and (b) solar potential is estimated by identifying available areas for solar panel installation. To affirm the efficacy of SolarNet+, we employ it on the RID dataset which is a benchmark dataset. Results show that SolarNet+ outperforms other competitors in terms of prediction accuracy of roof orientations and superstructures. Moreover, the transferability of SolarNet+ is also demonstrated by the results of the multi-task learning network which is trained using data from the RID dataset and then evaluated in an unseen city, Munich. Furthermore, we conduct an assessment of urban rooftop solar potential across various LCZ types, which is demonstrated using Brussels as a case study. Three LCZ types, including compact highrise (LCZ1), compact midrise (LCZ2), and heavy industry (LCZ10), collectively contribute to a higher potential for rooftop solar utilization. Urban planning and photovoltaic development strategies should prioritize the aforementioned LCZ types for development.

In this study, our method neglects the shading cast by neighboring buildings, which influences the actual energy generation. Three-dimensional (3D) data can contribute to estimating this factor [38]. For instance, the segmentation results from satellite images are merged with 3D city models to estimate rooftop solar potential by considering the shading effects of surrounding buildings [39,40]. Therefore, we are considering fusing 3D data and aerial imagery for this task in our future work. However, as city models are not yet available globally, deep learning approaches for estimating building height or even building inclination from aerial imagery could be leveraged to improve the solar potential analysis [41].

CRediT authorship contribution statement

Qingyu Li: Writing – review & editing, Writing – original draft, Visualization, Validation, Software, Methodology, Investigation, Formal analysis, Data curation, Conceptualization. **Sebastian Krapf:** Writing – review & editing, Visualization, Validation, Software, Methodology, Investigation, Formal analysis, Data curation. **Lichao Mou:** Writing – review & editing, Formal analysis. **Yilei Shi:** Writing – review & editing, Formal analysis. **Xiao Xiang Zhu:** Writing – review & editing, Resources, Project administration, Funding acquisition.

Declaration of competing interest

The authors declare the following financial interests/personal relationships which may be considered as potential competing interests: Xiaoxiang Zhu reports financial support was provided by German Federal Ministry of Education and Research. Xiaoxiang Zhu reports financial support was provided by German Research Foundation.

Data availability

Data will be made available on request.

Acknowledgments

The work is jointly supported by the Excellence Strategy of the Federal Government and the Länder through TUM Innovation Network EarthCare, by the German Federal Ministry of Education and Research (BMBF) in the framework of the international future AI lab “AI4EO – Artificial Intelligence for Earth Observation: Reasoning, Uncertainties, Ethics and Beyond” (grant number: 01DD20001), by German Federal Ministry for Economic Affairs and Climate Action in the framework of the “national center of excellence ML4Earth” (grant number: 50EE2201C) and by the Munich Center for Machine Learning.

References

- [1] United Nations. Sustainable development goal 11: Make cities inclusive, safe, resilient and sustainable. 2021, <https://www.un.org/sustainabledevelopment/cities/>. [Accessed: 16 Dec 2021].
- [2] IEA. Tracking clean energy progress 2023. 2023, <https://www.iea.org/reports/tracking-clean-energy-progress-2023>. [Accessed: 08 Feb 2024].
- [3] Gui E, Baldinelli G, Bartocci P, Bianchi F, Piergianni D, Cotana F, et al. A techno-economic analysis of a solar PV and DC battery storage system for a community energy sharing. Energy 2022;244:123191.
- [4] Joshi S, Mittal S, Holloway P, Shukla PR, Ó Gallachóir B, Glynn J. High resolution global spatiotemporal assessment of rooftop solar photovoltaics potential for renewable electricity generation. Nat Commun 2021;12(1):1–15.
- [5] Gassar AAA, Cha SH. Review of geographic information systems-based rooftop solar photovoltaic potential estimation approaches at urban scales. Appl Energy 2021;291:116817.
- [6] Aslani M, Seipel S. Automatic identification of utilizable rooftop areas in digital surface models for photovoltaics potential assessment. Appl Energy 2022;306:118033.
- [7] Kodysh JB, Omitaomu OA, Bhaduri BL, Neish BS. Methodology for estimating solar potential on multiple building rooftops for photovoltaic systems. Sustain Cities Soc 2013;8:31–41.
- [8] Held M, Ilg R. Update of environmental indicators and energy payback time of CdTe PV systems in Europe. Prog Photovolt: Res Appl 2011;19(5):614–26.
- [9] Mainzer K, Killinger S, McKenna R, Fichtner W. Assessment of rooftop photovoltaic potentials at the urban level using publicly available geodata and image recognition techniques. Sol Energy 2017;155:561–73.
- [10] Assouline D, Mohajeri N, Scartezzini J-L. Large-scale rooftop solar photovoltaic technical potential estimation using random forests. Appl Energy 2018;217:189–211.
- [11] Fogl M, Moudrý V. Influence of vegetation canopies on solar potential in urban environments. Appl Geogr 2016;66:73–80.
- [12] Huang Z, Mendis T, Xu S. Urban solar utilization potential mapping via deep learning technology: A case study of Wuhan, China. Appl Energy 2019;250:283–91.
- [13] Zhong T, Zhang Z, Chen M, Zhang K, Zhou Z, Zhu R, et al. A city-scale estimation of rooftop solar photovoltaic potential based on deep learning. Appl Energy 2021;298:117132.
- [14] Jiang H, Yao L, Lu N, Qin J, Liu T, Liu Y, et al. Geospatial assessment of rooftop solar photovoltaic potential using multi-source remote sensing data. Energy AI 2022;10:100185.
- [15] Lee S, Iyengar S, Feng M, Shenoy P, Maji S. Deeprof: A data-driven approach for solar potential estimation using rooftop imagery. In: ACM SIGKDD. 2019, p. 2105–13.
- [16] Faltermeier FL, Krapf S, Willenborg B, Kolbe TH. Improving semantic segmentation of roof segments using large-scale datasets derived from 3D city models and high-resolution aerial imagery. Remote Sens 2023;15(7):1931.
- [17] Li Q, Krapf S, Shi Y, Zhu XX. SolarNet: A convolutional neural network-based framework for rooftop solar potential estimation from aerial imagery. Int J Appl Earth Obs Geoinf 2023;116:103098.

- [18] Hafez A, Soliman A, El-Metwally K, Ismail I. Tilt and azimuth angles in solar energy applications—a review. *Renew Sustain Energy Rev* 2017;77:147–68.
- [19] Khan J, Arsalan MH. Estimation of rooftop solar photovoltaic potential using geo-spatial techniques: A perspective from planned neighborhood of Karachi–Pakistan. *Renew Energy* 2016;90:188–203.
- [20] Yang Y, Campana PE, Stridh B, Yan J. Potential analysis of roof-mounted solar photovoltaics in Sweden. *Appl Energy* 2020;279:115786.
- [21] Thai C, Brouwer J. Challenges estimating distributed solar potential with utilization factors: California universities case study. *Appl Energy* 2021;282:116209.
- [22] Ren H, Sun Y, Tse CFN, Fan C. Optimal packing and planning for large-scale distributed rooftop photovoltaic systems under complex shading effects and rooftop availabilities. *Energy* 2023;274:127280.
- [23] Krapf S, Kemmerzell N, Khawaja Haseeb Uddin S, Hack Vázquez M, Netzler F, Lienkamp M. Towards scalable economic photovoltaic potential analysis using aerial images and deep learning. *Energies* 2021;14(13):3800.
- [24] Krapf S, Bogenrieder L, Netzler F, Balke G, Lienkamp M. Rid—roof information dataset for computer vision-based photovoltaic potential assessment. *Remote Sens* 2022;14(10):2299.
- [25] Stewart ID, Oke TR. Local climate zones for urban temperature studies. *Bull Am Meteorol Soc* 2012;93(12):1879–900.
- [26] Zhou J, Yi Q, Wang Y, Ye Z. Temperature distribution of photovoltaic module based on finite element simulation. *Sol Energy* 2015;111:97–103.
- [27] Al-Ghezi MK, Ahmed RT, Chaichan MT. The influence of temperature and irradiance on performance of the photovoltaic panel in the middle of Iraq. *Int J Renew Energy Dev* 2022;11(2):501.
- [28] Huld T, Müller R, Gambardella A. A new solar radiation database for estimating PV performance in Europe and Africa. *Sol Energy* 2012;86(6):1803–15.
- [29] Ronneberger O, Fischer P, Brox T. U-Net: Convolutional networks for biomedical image segmentation. In: MICCAI. Springer; 2015, p. 234–41.
- [30] Srivastava S, Volpi M, Tuia D. Joint height estimation and semantic labeling of monocular aerial images with CNNs. In: IGARSS. 2017, p. 5173–6.
- [31] Bischke B, Helber P, Folz J, Borth D, Dengel A. Multi-task learning for segmentation of building footprints with deep neural networks. In: ICIP. 2019, p. 1480–4.
- [32] Mou L, Zhu XX. Vehicle instance segmentation from aerial image and video using a multitask learning residual fully convolutional network. *IEEE Tgrs* 2018;56(11):6699–711.
- [33] Chen L-C, Zhu Y, Papandreou G, Schroff F, Adam H. Encoder-decoder with atrous separable convolution for semantic image segmentation. In: ECCV. 2018, p. 801–18.
- [34] Jégou S, Drozdal M, Vazquez D, Romero A, Bengio Y. The one hundred layers Tiramisu: Fully convolutional densenets for semantic segmentation. 2017, p. 11–9, CVPR workshops.
- [35] Baheti B, Innani S, Gajre S, Talbar S. Eff-UNet: A novel architecture for semantic segmentation in unstructured environment. In: CVPR workshops. 2020, p. 358–9.
- [36] Li M-F, Tang X-P, Wu W, Liu H-B. General models for estimating daily global solar radiation for different solar radiation zones in mainland China. *Energy Convers Manag* 2013;70:139–48.
- [37] Demuzere M, Kittner J, Martilli A, Mills G, Moede C, Stewart ID, et al. A global map of local climate zones to support earth system modelling and urban scale environmental science. *Earth Syst Sci Data Discuss* 2022;2022:1–57.
- [38] Krapf S, Willenborg B, Knoll K, Bruhs M, Kolbe TH. Deep learning for semantic 3d city model extension: Modeling roof superstructures using aerial images for solar potential analysis. *ISPRS Ann* 2022;10.
- [39] Ren H, Xu C, Ma Z, Sun Y. A novel 3D-geographic information system and deep learning integrated approach for high-accuracy building rooftop solar energy potential characterization of high-density cities. *Appl Energy* 2022;306:117985.
- [40] Ren H, Ma Z, Chan AB, Sun Y. Optimal planning of municipal-scale distributed rooftop photovoltaic systems with maximized solar energy generation under constraints in high-density cities. *Energy* 2023;263:125686.
- [41] Li Q, Mou L, Hua Y, Shi Y, Chen S, Sun Y, et al. 3DCentripetalNet: Building height retrieval from monocular remote sensing imagery. *Int J Appl Earth Obs Geoinf* 2023;120:103311.